Vehicle Tracking and Motion Prediction in Complex Urban Scenarios

Christoph Hermes, Julian Einhaus, Markus Hahn, Christian Wöhler and Franz Kummert

***Abstract*— The recognition of potentially hazardous situations on road intersections is an indispensable skill of future driver assistance systems. In this context, this study focuses on the task of vehicle tracking in combination with a long-term motion prediction (1–2 s into the future) in a dynamic scenario. A motion-attributed stereo point cloud obtained using computationally efficient feature-based methods represents the scene, relying on images of a stereo camera system mounted on a vehicle. A two-stage mean-shift algorithm is used for detection and tracking of the traffic participants. A hierarchical setup depending on the history of the tracked object is applied for prediction. This includes prediction by optical flow, a standard kinematic prediction, and a particle filter based motion pattern method relying on learned object trajectories. The evaluation shows that the proposed system is able to track the road users in a stable manner and predict their positions at least one order of magnitude more accurately than a standard kinematic prediction method.**

I. Introduction

Future driver assistance systems will have to be able to interpret complex traffic situations and will therefore have to estimate and predict the position and motion state of the ego-vehicle and other vehicles surrounding it over time intervals of several seconds. Such information will e.g. allow to assess the risk of an upcoming situation.

A long-term prediction method requires adequate motion history knowledge for each vehicle in the scene. Especially for noisy 3D point data from a stereo camera system (cf. Fig. 1(b)) the application of a tracking method is favourable for minimising the effects of noise over time. It is common to use a Kalman filter approach [1] with a manually defined motion model for the prediction part, but this approach often lacks adaptation speed when the object rapidly changes its driving behaviour. Instead, we apply a modification of the particle filter framework proposed in [2], where the motion model is defined by recorded motion patterns, and extend this method by the simultaneous detection of several objects, such that the particle filter is able to track several motion hypotheses for each traffic participant in parallel.

For this contribution, we have chosen a roundabout as a test scenario as it includes several different motion patterns normally found in urban traffic: For traffic participants at large distances to the sensor (about 30–50 m), small errors in the stereo point cloud computation lead to a considerable amount of noise [3]. Additionally, the vehicles often occlude each other. Objects passing by in front of the camera are visible only for short periods of time, about 3–4 s. In this case, a tracking algorithm based on temporal filtering has very little time to settle its parameters. Turning vehicles yield high dynamics compared to a simple turn at intersections, which tends to be difficult to follow for a standard filter.

(a) Left image from stereo camera setup.

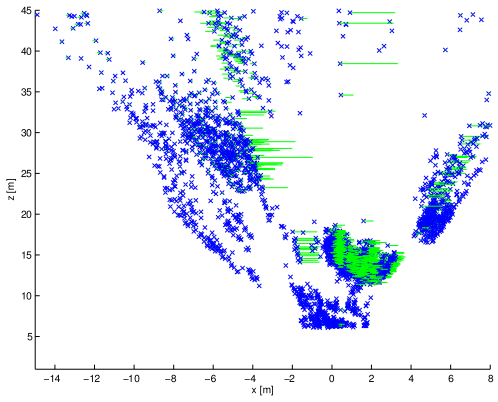

(b) Corresponding motion-attributed 3D point cloud (top view).

Fig. 1. Roundabout scenario.

The issue of vehicle tracking has been addressed by many researchers in the past decades and a complete overview would be out of the scope of this paper. For the interested reader in the field of object tracking in general, we refer to the excellent surveys by Lepetit and Fua [4] and by Yilmaz et al. [5]. Numerous works in the domain of vehicle tracking deal with the Kalman filter approach [1] and its common extensions like the Extended Kalman filter (EKF)

C. Hermes and F. Kummert are with the Faculty of Technology, Bielefeld University, Bielefeld, Germany, {chermes, franz}@techfak.uni-bielefeld.de

J. Einhaus and M. Hahn are with Daimler AG, Group Research, Ulm, Germany, {Julian.Einhaus, Markus.Hahn}@daimler.com

C. Wöhler is with the Image Analysis Group, Dortmund University of Technology, Dortmund, Germany, christian.woehler@tu-dortmund.de

or the Unscented Kalman filter (UKF). Various features are used for tracking. Melli et al. [6] detect stopping vehicles with two-dimensional boxes in images based on an extension of the Kalman filter. Background and shadow classification are handled separately. A multiple filter setup is used by Barth and Franke [7], where each three-dimensional object point is assigned an individual Kalman filter and is tracked over time. A vehicle is represented by such a point cloud and segmented based on a cuboid model. Active contours and silhouettes are also widely used for vehicle tracking. Yokoyama and Poggio [8] combine edge features and optical flow for object tracking with active contours. Similarly, Luo and Bhandarkar [9] present a tracking approach based on regions and contours, where velocity fields are used in order to approximate the object contour by B-spline surfaces combined with a Kalman filter.

Other works in the field of vehicle tracking include the tracking-by-detection method [3] and tracking of non-parametric probability densities. For example, Comaniciu et al. [10] use histograms together with a mean-shift algorithm on RGB color features to track people in dynamic scenes. Heisele [11] uses colour and optical flow features for tracking clusters in images. These clusters are used to form motion trajectories for generating object hypotheses. Schiele [12] finds homogeneous regions in images by using a k-means clustering in color space. Objects or object parts are combined and tracked with a Viterbi-based tracking algorithm for similarly moving regions. A vehicle tracking method based on 3D models is presented in [13], [14]. Relying on the association of edge elements and optical flow, the models are applied to vehicles appearing small in images acquired with a traffic surveillance camera. Support Vector Machines (SVMs) are used by Avidian [15] for a stable tracking of vehicle rear ends in traffic. The classification is performed in images taken with a monocular camera mounted on the ego-vehicle.

Hidden Markov Models (HMMs) are another well-established state estimation and tracking method for vehicles. Fraile and Maybank [16] estimate discrete states of the vehicle for classifying the movement of the tracked object. Yin et al. [17] use a HMM for vehicle part detection and track them in congested traffic over time.

A few researchers have addressed the topic of vehicle state prediction based on previously observed motion patterns: Johnson and Hogg [18] represent a set of pedestrian trajectories using a neural network combined with vector quantisation. They suggest an event recognition and prediction method using probability densities which are determined by the distribution of the prototype vectors. Sumpter et al. [19] propose a long-term spatio-temporal prediction method for a flock of animals in the presence of a predator based on observed trajectories and flock shapes. Similar to [18], the authors utilise a neural network combined with vector quantisation to cluster the motion data. The prediction is performed by a recursive loop where in each iteration the winning neuron is predicted into the next time step by the network. Hu et al. [20] determine image-based trajectories of vehicles

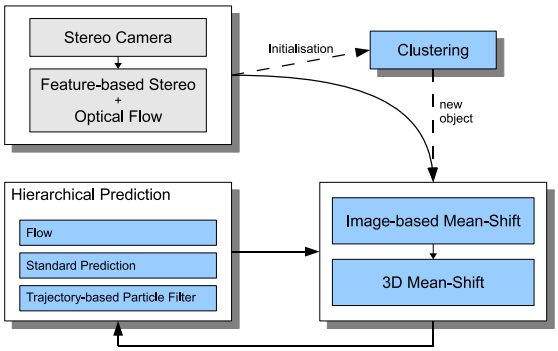

Fig. 2. System overview.

using foreground classification and a exponential smoothing-based prediction method. A hierarchical clustering algorithm is applied to retrieve typical motion patterns from a given set of trajectories. Each motion pattern is represented by a chain of Gaussian distributions which are used for statistical anomaly detection and behaviour prediction.

An overview of the tracking and prediction method proposed in this study is shown in Fig. 2. A 3D bounding box model represents a vehicle in the scene (cf. Section II). The environment of the observer is represented by a motion-attributed 3D point cloud. New objects entering the scene are detected by graph-based clustering and verified for further time steps by a two-step mean-shift algorithm (cf. Section III). For tracking, we apply a hierarchical prediction method depending on the length of the observed motion history (cf. Section IV). The tracking and long-term prediction approaches are evaluated quantitatively in Section V.

II. Object and Motion Model

The ego-vehicle observes the environment with a stereo camera sensor. Each traffic participant (e.g. vehicles and bicycles) is assumed to be a rigid object, i.e. shape deformations do not occur during tracking. Pedestrians are not considered in the proposed method because their motion is difficult to predict even by a human driver. An object is represented as a three-dimensional bounding box $\Phi = [c_x, c_z, s_x, s_y, s_z]^T$ covering the rough shape of the object. The dimensions x, y and z denote the lateral, elevation, and longitudinal axis, respectively, according to the camera coordinate system. The box model includes the projected centre $\mathbf{c} = [c_x, c_z]^T$ to the ground and is aligned parallel to the image plane of the camera system. Therefore the object dimension $[s_x, s_y, s_z]^T$ denotes the spatial extension according to the camera coordinate axes.

In this study, motion patterns from a training set are compared with the observed history of a tracked object. Similar to [2], a motion pattern is represented as a trajectory T which consists of ordered tuples $T = ((\Phi_{(1)}, t_1), \ldots, (\Phi_{(N)}, t_N))$. This combines the object state $\Phi_{(\mathrm{id})}$ with a time stamp $t_{(\mathrm{id})}$. The object orientation (yaw angle) and higher derivatives like the yaw rate and velocity can be inferred from the first two dimensions of the object state Φ over time by numerical computation of the temporal derivatives.

III. Object Detection

The idea behind the tracking system is to extract the motion patterns of all moving objects in the observed scene. For this purpose their 3D positions and motion states have to be estimated (cf. Section III-A). We use a standard stereo two-camera setup with a baseline of 220 mm for three-dimensional environment perception. The stereo camera system is calibrated and the images are rectified to standard epipolar geometry. When a vehicle enters the scene, the proposed system sets up a new tracking model based on an initially detected object (cf. Section III-B). Additionally, the system generates a "target model" for tracking the object both in the camera images (image-based mean-shift, cf. Section III-C) and in the 3D point cloud (point cloud-based mean-shift, cf. Section III-D).

A. Sparse Scene Flow

Object detection and 3D tracking are based on a sparse scene flow field. We use a combination of sparse correlation-based stereo and sparse optical flow. Both algorithms are based on the computationally efficient correspondence estimation method described by Stein [21], where corresponding feature points in the images of the left and the right camera are used to obtain the 3D points and the current and previous camera images are used to compute the optical flow field.

The optical flow field vectors are assigned to the 3D points by computing the mean velocity in a small neighbourhood (2 pixels radius) of the spatial points in the image plane. This results in a motion-attributed point cloud, better known as the scene flow field (Fig. 3(a)). Therefore, each scene flow point $\mathbf{s}_i = [s_{i,x}, s_{i,y}, s_{i,z}, \dot{s}_{i,x}, \dot{s}_{i,y}]^T$ has a spatial part $[s_{i,x}, s_{i,y}, s_{i,z}]^T$ and a velocity part $[\dot{s}_{i,x}, \dot{s}_{i,y}]^T$. In contrast to classical scene flow [22], the longitudinal velocity part $\dot{s}_{i,z}$ of the stereo points is not determined. This drawback is compensated by the high computational efficiency of the correspondence estimation method.

A graph based clustering algorithm according to [23] is used to separate differently moving groups of 3D points from each other. First the moving objects are separated from the stationary ones by taking only those points from the scene flow point set $S = \{\mathbf{s}_1, \ldots, \mathbf{s}_M\}$ with a velocity $\|[\dot{s}_{i,x}, \dot{s}_{i,y}]^T\| > \varepsilon_v$ relative to the stationary environment, which results in a reduced scene flow point set $S_{\varepsilon_v} \subseteq S$. Objects standing still when entering the sensors field of view will be considered as stationary objects. A cluster $A \subseteq S_{\varepsilon_v}$ can be defined as a point set with maximum similarity whereas the similarity between different clusters is minimised. For each point $\mathbf{s}_i \in S_{\varepsilon_v} \backslash A$ a δ-vicinity exists such that $\mathbf{s}_i$ is added to A if $\exists \mathbf{s}_j \in A \colon d(\mathbf{s}_j, \mathbf{s}_i) < \delta$, where $d(\cdot,\cdot)$ denotes the Euclidean distance metric and δ is a distance threshold. This procedure is repeated for all $\mathbf{s}_i \in S_{\varepsilon_v}$ until no point can be added to A any more. The next clusters are computed correspondingly. For illustration, the colour of each 3D point in Fig. 3(b) is chosen according to its cluster assignment.

Tracked vehicles may reduce their speed or stop completely, especially at intersections. Hence, a cluster will not always be detected, such that it cannot be used as the only tracking feature. We therefore use the image grey values as additional tracking features.

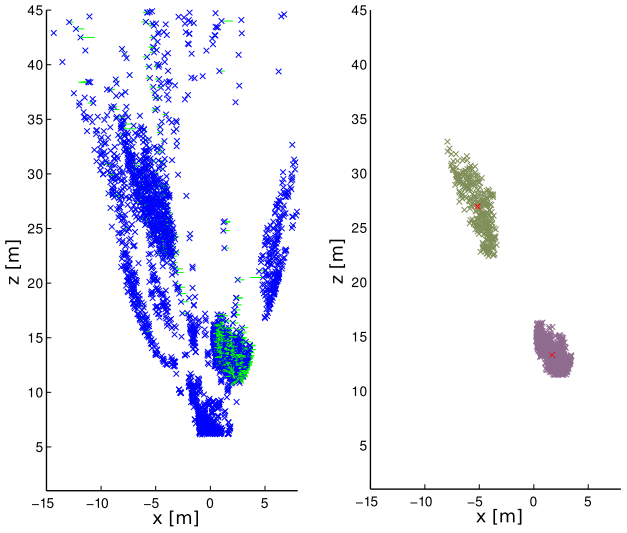

(a) 3D point cloud (blue) and assigned velocities (green).

(b) Clustering result.

Fig. 3. Scene flow and clustering result (top view).

B. Model Initialisation

For each object in the scene, the tracking system requires an initial pose. This step is necessary when a previously unseen object enters the scene or when the track is lost because of multiple mutual occlusions, such that the object appears at unexpected locations. For this purpose we apply the clustering method at each time step: When a cluster is found which cannot be assigned to an existing tracked object, i.e. the distance value exceeds a threshold d_{obj}, a new model $\Phi_{(\text{id})}(t_0)$ is set for this cluster and tracked over the following time steps $t > t_0$. The cluster centre projected to the ground serves as the model centre and the initial model dimensions are determined by a bounding box around a cluster.

As mentioned before, the cluster method is not suitable to serve as the only tracking feature due to the fact that clusters are missing over several frames. In addition, the objects are tracked both in the camera images and in the original point cloud, where the image grey values are used to weight each 3D point. This weighting is based on a target model $\hat{\mathbf{q}}_{(\text{id})}$ for each object (id) consisting of a grey value histogram with 256 bins. Assuming that all three-dimensional points on the model $\Phi_{(\text{id})}$ have the same depth value, a three-dimensional model projection onto the camera images simplifies to the projection of a parallel plane. This means that each visible three-dimensional model point can be projected efficiently into the camera images. The histogram $\hat{\mathbf{q}}_{(\text{id})}$ is first computed by the projection of the initial model $\Phi_{(\text{id})}(t_0)$ into each camera image and is updated incrementally in the following time steps using

$$\hat{\mathbf{q}}'_{(\text{id})}(t+1) = \alpha \cdot \hat{\mathbf{q}}_{(\text{id})}(t) + (1-\alpha) \cdot \hat{\mathbf{q}}_{(\text{id})}(t+1). \qquad (1)$$

The target model is normalised such that $\sum_{j=1}^{256} \hat{q}_i^{(j)} = 1$ and

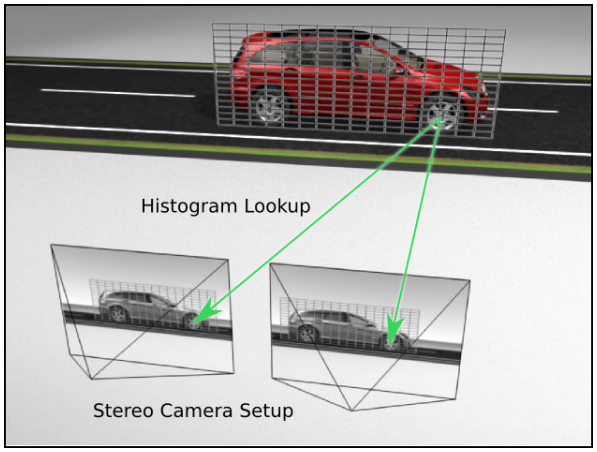

Fig. 4. Image-based mean-shift: 3D grid parallel to stereo image layers. Each grid cell is projected into the stereo images and weighted with the corresponding grey values.

is interpreted as an occurrence probability for each grey value. An image-based mean-shift algorithm looks for the most likely image region in the following time steps by comparing the grey value histograms. Since the histogram contains no spatial information, the object tracking is robust against object rotations and illumination changes.

C. Image-based Mean-shift

A target model $\hat{\mathbf{q}}_{(\mathrm{id})}(t)$ of the corresponding object model $\Phi_{(\mathrm{id})}(t)$ is used to guide a mean-shift algorithm inside a search window to the object centre. This method is based on the CAMShift algorithm proposed by Bradski [24], but instead of specifying the search window to be in image coordinates, we look for the mean object centre in 3D space by defining a grid parallel to the image plane as shown in Fig. 4. The three-dimensional cell size of the grid corresponds to the projected pixel size in both camera images. For each grid cell $\mathrm{gCell}_i(\mathbf{x}_i)$ with mean centre $\mathbf{x}_i$ an intensity value is assigned by projecting $\mathbf{x}_i$ into both camera images $\mathbf{I}_{(1,2)}$, yielding the image coordinates $\mathbf{u}_i$, and taking the mean grey value:

$$\mathrm{gCell}_i(\mathbf{x}_i) = \frac{1}{2}[\mathbf{I}_1(\mathbf{u}_i) + \mathbf{I}_2(\mathbf{u}_i)]. \tag{2}$$

A look-up in the target model histogram results in an occurrence probability $\hat{\mathbf{q}}_i(\mathrm{gCell}_i)$ for each grid cell gCell_i.

The 3D centre point $\tilde{\mathbf{c}}$ is estimated with the mean-shift procedure using a geometric rectangle model. This mean-shift state allows only for an update of the lateral pose of the tracked object, since the probability grid is parallel to the image plane. No information from the scene flow field is used, such that a pose update of the rectangle is computed even if there is no new 3D information available.

D. Point Cloud based Mean-shift

In this stage all moving 3D points of the scene flow field are used to update the 3D pose of the tracked box. At the first iteration $j = 1$ of the mean-shift procedure the box centre $\mathbf{c}_{j=1}$ is initialised with the estimated 3D centre point $\tilde{\mathbf{c}}$ of the image-based mean-shift stage. For all subsequent iterations, the box model is moved to the new position

$$\mathbf{c}_{j+1} = \frac{\sum_{n=1}^{N} \mathbf{s}_n \cdot g(\mathbf{s}_n, \mathbf{c}_j) \cdot \hat{\mathbf{q}}_{(\mathrm{id})}(\mathrm{gCell}_i(\mathbf{s}_n))}{\sum_{n=1}^{N} g(\mathbf{s}_n, \mathbf{c}_j) \cdot \hat{\mathbf{q}}_{(\mathrm{id})}(\mathrm{gCell}_i(\mathbf{s}_n))} \tag{3}$$

where $\mathbf{c}_j$ is the previous centre position. In the mean-shift procedure we use a truncated Gaussian kernel [25]

$$g(\mathbf{s}_n, \mathbf{c}_j) = \begin{cases} e^{-\beta ||\mathbf{s}_n - \mathbf{c}_j||^2} & \text{if } ||\mathbf{s}_n - \mathbf{c}_j||^2 \leq \lambda \\ 0 & \text{otherwise} \end{cases} \tag{4}$$

where β denotes the kernel width and λ defines the maximum allowed distance of $||\mathbf{s}_n - \mathbf{c}_j||^2$ and is typically chosen such that $\int_0^{\lambda} e^{-\beta ||\mathbf{s}_n - \mathbf{c}_j||^2}$ covers 99% of the area under the Gaussian kernel function.

Our mean-shift based 3D tracking approach incorporates an appearance weighting $\hat{\mathbf{q}}_{(\mathrm{id})}(\mathrm{gCell}_i(\mathbf{s}_n))$ obtained by looking up the appearance probability of the moving 3D point $\mathbf{s}_n$ in the target model $\hat{\mathbf{q}}_{(\mathrm{id})}$, such that a 3D point with an appearance similar to the target appearance is assigned a higher weight.

IV. Object Tracking

For a driver assistance system not only the position of other traffic participants but also their future behaviour is important, i.e. where the other objects will be in the subsequent time steps. In this context, our previous work [2] presents a long-term (~ 2 s ahead) behaviour prediction method, but it is assumed that a motion history (≥ 30 frames) has already been observed. This assumption cannot be directly applied here, because new objects entering the scene have no observed motion history. Therefore, we extend the work in [2] by a hierarchical prediction method whose application depends on the length of the motion history. For newly detected objects a simple flow-based prediction is applied (cf. Section IV-A). Once the history length of a tracked object exceeds a predefined threshold l_1 we use a so-called kinematic prediction (cf. Section IV-B), which yields the approximate motion direction. Similarly, the trajectory-based prediction method (cf. Section IV-C) is applied when the history length is larger than a threshold l_2 with $l_2 > l_1$ and is used for the prediction step in the tracking system as well as for a long-term prediction of the object state. In general, the prediction becomes more stable with increasing length of the motion history.

For each traffic participant a new tracker instance is created when the system detects an object. Because the stereo cameras have a similar field of view as the driver, mutual occlusions between the traffic participants often occur. Especially when an object passes a row of vehicles in the rear area of the observed scene, the object cannot be found by the detector. Therefore we set an occlusion flag when an object is hidden, which causes the tracker to disable the object detection step for the corresponding frame.

A. Flow-Based Prediction

The flow-based prediction utilises the velocity information from the scene flow field. An object $\Phi_{(\mathrm{id})}(t-1)$ is predicted to the current time step t using the linear equation

$$\Phi_{(\mathrm{id})}(t) = \Phi_{(\mathrm{id})}(t-1) + [\tilde{\mathbf{v}}_i \cdot \Delta t, 0, 0, 0]^T, \tag{5}$$

where $\tilde{\mathbf{v}}_i$ is the median velocity of all scene flow points $\mathbf{s}_i$ inside the box model $\Phi_{(\mathrm{id})}(t-1)$ and Δt denotes the time difference between two successive frames. Zero values in (5) indicate the absence of change in the box model dimensions. Note that $\tilde{\mathbf{v}}_i$ is a two-dimensional vector parallel to the camera image planes because the optical flow yields no depth information. It is assumed that the point cloud based mean-shift can handle the depth adjustment sufficiently well.

B. Kinematic Prediction

The kinematic prediction is an extrapolation technique assuming constant acceleration and curve radius with respect to the current vehicle state. This prediction yields a circular path on which the vehicle performs a constantly accelerated motion. Although the acceleration based on the tracked object path is sensitive to noise, the curve radius has more influence on the kinematic prediction model since it affects the motion direction. This simple kinematic model allows good predictions for time intervals of a few tenths of a second but yields unrealistic and inaccurate results when performing a long-term prediction for time intervals of several seconds.

C. Trajectory Particle Filter

The trajectory-based prediction utilises a set of previously observed motion patterns (i.e. reference trajectories) and finds the most probable hypotheses (sub-trajectories) to represent the current object motion history based on the longest common subsequence (LCS) [26]. Each hypothesis is weighted by the quaternion-based rotationally invariant longest common subsequence (QRLCS) metric [2]. This metric compares the difference between two trajectories and finds the best matching subsequence in each compared trajectory while preserving the optimal transformation (rotation and translation in the 2D plane) of one sub-trajectory to the other.

The LCS can be computed with the dynamic programming (DP) algorithm using tables in which partial (optimal) results of the algorithm are stored. The optimal, partial translation and rotation is obtained by regarding the trajectories as two point sets in which the point-to-point assignments are given by the DP table. Hence, the rotation angle and the mean values for each point set are computed incrementally.

The best translation of a trajectory A to a trajectory B can be obtained using the mean values μ_a and μ_b. The mean μ_a of point set $\{\mathbf{a}_i\}$ is computed incrementally by

$$\mu_{a,T} = \frac{(T-1)}{T}\,\mu_{a,T-1} + \frac{1}{T}\,\mathbf{a}_T \tag{6}$$

with T as the number of point assignments (analogous for point set $\{\mathbf{b}_i\}$). For the optimal rotation, a closed-form solution for the least-squares problem of absolute orientation with quaternions is given in [27]. A quaternion can be considered as a complex number with three different imaginary parts or the combination of a scalar with a 3D Cartesian vector, $\dot{\mathbf{q}} = q_0 + iq_x + jq_y + kq_z \equiv [q_0, \mathbf{q}]$. It can be used as a rotation operator on a three-dimensional vector $\mathbf{x}$ according to $[0, \mathbf{x}^R] = \dot{\mathbf{q}}[0, \mathbf{x}]\dot{\mathbf{q}}^{-1}$, where vectors are treated as quaternions with zero scalar component. A rotation quaternion can be constructed based on the rotation angle θ and the three-dimensional rotation vector $\mathbf{n}$:

$$\dot{\mathbf{q}} = \sqrt{\frac{1+\cos\theta}{2}} + \frac{\sin\theta}{\sqrt{2(1+\cos\theta)}}(in_x + jn_y + kn_z) \tag{7}$$

Because of the reasonable flat-world assumption the rotation vector can be set to the fixed value $\mathbf{n} = [0, 0, 1]$. For the rotation in a plane, the rotation vector is constructed in [27] from two given point sets using

$$\sin\theta = S/\sqrt{S^2 + C^2} \qquad \cos\theta = C/\sqrt{S^2 + C^2}. \tag{8}$$

By rotating the point sets (trajectories) up to an assignment T around their mean centres $\mu_{a,T}$ and $\mu_{b,T}$, the auxiliary variables S and C become

$$S_T = \left\langle \left(\sum_{t=1}^{T} (\mathbf{a}_t \times \mathbf{b}_t) - T(\mu_{a,T} \times \mu_{b,T}) \right), \mathbf{n} \right\rangle \tag{9}$$

$$C_T = \sum_{t=1}^{T} \langle \mathbf{a}_t, \mathbf{b}_t \rangle - T \left\langle \mu_{a,T}, \mu_{b,T} \right\rangle, \tag{10}$$

where $\langle \cdot, \cdot \rangle$ and $\times$ denote the dot product and the cross product, respectively. As a result, only the incremental parts $\mu_{a,T}$ and $\mu_{b,T}$ (Eq. (6)), $\sum_{t=1}^{T}(\mathbf{a}_t \times \mathbf{b}_t)$ (Eq. (9)), and $\sum_{t=1}^{T}\langle \mathbf{a}_t, \mathbf{b}_t \rangle$ (Eq. (10)) have to be stored for each assignment test in the DP table to guarantee the best rotation and translation.

Similar parts of the reference trajectories are taken as hypotheses and tracked over time by a particle filter framework. The prediction step is then a simple lookup in the future trajectory point of the corresponding hypothesis. This results in multiple object state predictions, where for a single prediction the mean value of the predictions of all hypotheses is taken. This method is also applied to obtain predictions for longer time intervals into the future.

The reference trajectories incorporate all information about the object state Φ at each trajectory element. For this reason there is no need for an explicit motion model since the observed trajectories also cover the state noise. This set of motion patterns is obtained by tracking traffic participants while they are inside the field of view without using the trajectory-based prediction step.

V. Evaluation

The evaluation of the proposed tracking system is based on eight sequences of rectified stereo image pairs of a roundabout. Each sequence is recorded with a frame rate of 42.0 ms/frame and has an approximate length of 250 frames. To be able to track such relatively long sequences, the observing vehicle with the mounted stereo camera system stands in front of the roundabout. For a moving vehicle, ego-motion compensation e.g. according to [7] would have to be

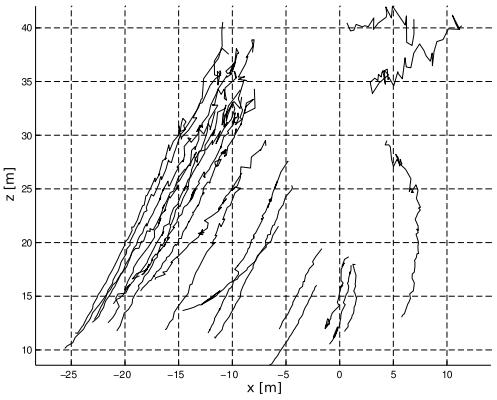

Fig. 5. Motion patterns extracted by our approach.

applied. We take six sequences for motion pattern extraction from non-occluded traffic participants for the training set of the trajectory-based particle filter. The remaining two sequences (in the following labelled as A and B) are used for testing and contain 1127 object positions to be tracked in 500 frames. The motion pattern extraction makes use of the previously described two-stage mean-shift algorithm with the flow-based and kinematic prediction method. This results in 44 trajectories (cf. Fig. 5) for the training set. Each trajectory point represents the box model ϕ_i.

In the tracking system, we use an update rate $\alpha = 0.2$ (Eq. (1)), a velocity threshold $\varepsilon_v = 2.3$ m/s for clustering, and a δ-vicinity value of 0.5 m. We set the Gaussian kernel width to $\beta = 0.8 \cdot \min\{s_x, s_y, s_z\}$, i.e. its value depends on the tracked object dimension. In the hierarchical prediction method, we apply the flow-based prediction if the trajectory history is shorter than 5 frames (0.21 s), the kinematic prediction is applied to a trajectory history in the range 5–30 frames (0.21–1.26 s), and the particle filter is used for history lengths ≥ 30 frames (1.26 s) with 200 particles, where only the last 30 frames are taken into account.

The evaluation consists of two parts, where first the tracking performance is compared with manually labelled ground truth, and then the prediction capability for several time steps ahead is shown for the trajectory particle filter.

A. Tracking Results

3D ground truth of the objects in the scene is not available, i.e. their distance to the camera is unknown. For an adequate quality assessment of the proposed tracking system, the object positions are labelled manually as bounding boxes, resulting in the centre of the object and its dimensions in the two-dimensional image plane. The 3D object model $\Phi_{(\mathrm{id})}$ detected by the tracking system is then projected into the camera images and compared with the manually labelled boxes. At time step t, we define the tracking quality as a function of the overlap in the horizontal direction according to

$$E(\Phi_{(\mathrm{id})}(t), \mathbf{O}_{(\mathrm{id})}(t)) = \begin{cases} 1 & \text{if } \frac{\mathrm{overlap}(\mathbf{O}_{(\mathrm{id})}(\mathrm{t}), \Phi_{(\mathrm{id})}(\mathrm{t}))}{\min\{\mathrm{w}(\mathbf{O}_{(\mathrm{id})}(t)), \mathrm{w}(\Phi_{(\mathrm{id})}(t))\}} > \varepsilon_o \\ 0 & \text{otherwise,} \end{cases} \tag{11}$$

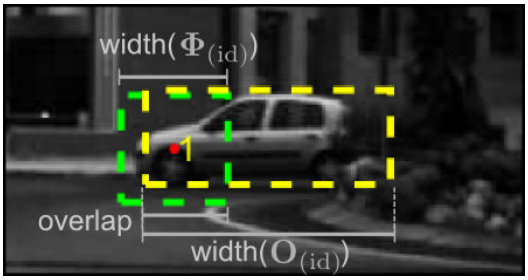

Fig. 6. Tracking quality function example for a manually labelled object $\mathbf{O}_{(\mathrm{id})}$ (yellow) and a tracked object $\Phi_{(\mathrm{id})}$ (green).

where $\mathbf{O}_{(\mathrm{id})}$ is the manually assigned ground truth of the tracked object $\Phi_{(\mathrm{id})}$, overlap$(\cdot,\cdot)$ denotes the horizontal overlap in pixel units of the boxes, and w$(\cdot)$ is the horizontal dimension (width) of the bounding box in image coordinates. The overlap threshold ε_o is set to 0.1. An example is depicted in Fig. 6. The tracking results differ depending on the kind of motion at the roundabout as mentioned in the introduction. We divide our test set of motion trajectories into three categories depending on their general motion type (cf. Fig. 7):

- **Category I**: Objects which enter the roundabout $\sim$40–50 m ahead in the left side of the image and drive closely along the observing vehicle by moving towards the right side of the image. (6 cars, 1 cyclist)
- **Category II**: Objects driving from the right to the left side $\sim$ 35 m ahead. (8 cars)
- **Category III**: Objects which enter the scene on the right side of the image and follow the path through the roundabout. (3 cars)

We evaluate the proposed tracking system in each category and in both test sequences A and B for two prediction methods. The objects are tracked over time by the flow-based and kinematic prediction method ("kin." in Table I) and by all predictions methods, including the trajectory particle filter (PF). Table I shows the median tracking percentage per object with the corresponding 25% and 75% quantiles.

Between the categories and sequences there is no major difference in the median tracking result. However, using the trajectory particle filter method often leads to a reduction of the tracking error, which means that the objects are tracked in a more stable manner. In sequence B, the objects of category II cannot be tracked. This is due to the fact that especially in this sequence objects are occluded by objects from category I most of the time, which means that the tracking system is not able to build up a stable motion history, such that hardly any measurements are provided by the object detection stage and no sufficiently long motion history is available for a stable tracking.

In sequence A, objects of category I are tracked only half of the time they are present in the scene for both prediction approaches used in the tracking system. In this case, a queue of cars enters from the left hand side at a distance of approximately 40 m, where the cars follow

Fig. 7. Motion categories I–III.

TABLE I
TRACKING RESULTS.

category	sequence	prediction method	median [%]	quantiles 25%	quantiles 75%
I	A	kin.	52.7	−1.5	+23.3
		PF	51.6	−0.7	+0.8
	B	kin.	94.2	−16.2	+5.1
		PF	99.2	−17.1	+0.9
II	A	kin.	79.7	−9.1	+8.4
		PF	83.8	−1.7	+8.2
	B	kin.	–	–	–
		PF	–	–	–
III	A	kin.	93.5	–	–
		PF	94.8	–	–
	B	kin.	98.7	−1.4	+1.4
		PF	98.7	−1.4	+1.4

each other closely. Because of the noise of the scene flow at this distance from the camera, the clustering stage is not capable of distinguishing between the similarly moving objects before the objects have moved to a point in the middle between their entrance point and the camera position. But once the tracking system is initialised on an object, the trajectory-based particle filter is able to track the object in a somewhat more stable manner than the tracking system with the kinematic prediction.

B. Prediction Results

In the evaluation of the long-term prediction we compare the prediction capability of the trajectory particle filter system with the kinematic prediction for several time intervals ahead (0.2 s, 0.6 s, 1.0 s, and 1.5 s). As a ground truth, we use the complete trajectories of tracked objects estimated by the proposed tracking framework with a tracking performance $> 90\%$ without using the particle filter based prediction. This ground truth is not completely independent of the tracking system, but we assume a minor influence on the prediction behaviour for several frames (time steps of 42 ms) ahead. To be precise, one object is tracked over time and the resulting trajectory is used as a ground truth for the long-term prediction methods, which estimates the future object position at each time step. Because only the manually verified object positions are adopted and mutual occlusions of the objects often occur, this ground truth is not complete but has several "gaps" which are ignored in the evaluation. The prediction error is determined by computing

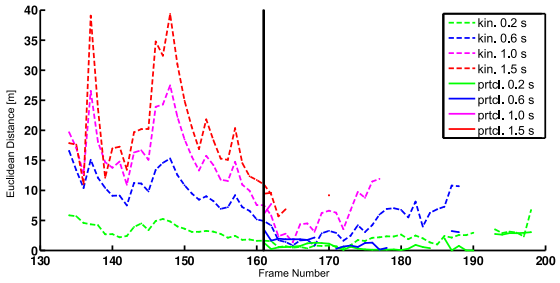

(a) Tracked object of category I.

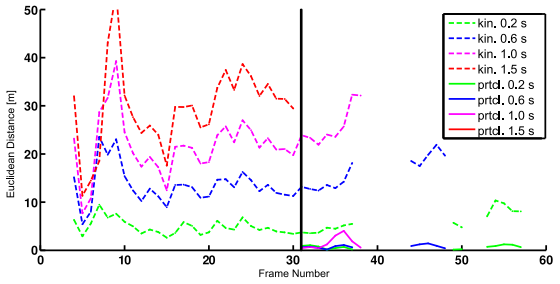

(b) Tracked object of category II.

Fig. 8. Long-term prediction error for different time intervals with kinematic prediction ("kin.") and trajectory-based particle filter prediction ("prtcl.").

the Euclidean distance of the predicted position and the ground truth position projected on the ground.

The long-term prediction errors are shown in detail for two object tracks in Fig. 8 for different prediction intervals. Figure 8(a) shows an object assigned to category I, whereas the object of Fig. 8(b) belongs to category II. The vertical line denotes the minimum history length (30 frames) for the particle filter to operate. Thus, only starting from that moment in time, prediction results exist for the trajectory particle filter. In both figures the error of the position predicted by the particle filter system is considerably smaller than the one inferred from the position predicted by the kinematic prediction method. Due to the noise in the history computed by the tracking system, the kinematic prediction is not able to determine the current object position very accurately, which would be required to obtain reasonable values for the current acceleration and curve radius. Therefore, the kinematic prediction often oscillates around the ground truth, leading to a high error compared to the trajectory-based prediction which already incorporates the measurement noise in the trajectories.

Since the particle filter is based on the Bayes filter algorithm [28], it needs a few time steps to consolidate a previously given random particle distribution to an estimated mode with little variance. As Fig. 9 suggests, showing an object driving aross a roundabout, this consolidation is achieved by the particle filter system within $\sim$ 2–5 frames.

Table II summarises the mean prediction errors for different prediction intervals for the two test sequences (500 frames) with 20 object trajectories. The difference between the prediction errors of the kinematic and the

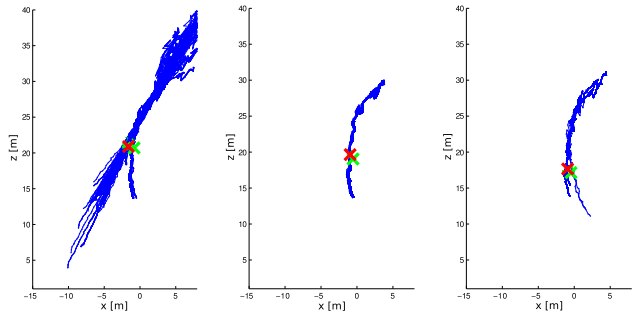

(a) Frame 162, $t = 0.0$ s (b) Frame 166, $t = 0.1$ s (c) Frame 171, $t = 0.3$ s

Fig. 9. Particles (blue) for a vehicle driving across a roundabout. The estimated vehicle position (red) is compared with the true position (green).

TABLE II

MEAN PREDICTION ERROR FOR DIFFERENT PREDICTION INTERVALS.

	prediction interval			
	0.2 s	0.6 s	1.0 s	1.5 s
kinematic prediction	4.2 m	9.8 m	13.8 m	16.9 m
particle filter	0.6 m	1.3 m	4.2 m	9.5 m

trajectory-based prediction grows significantly with increasing prediction interval. For each regarded prediction interval, the trajectory-based particle filter is clearly superior to the kinematic prediction but still needs further improvements for a prediction horizon ≥ 1.0 s especially for dense traffic scenarios.

VI. SUMMARY AND CONCLUSION

In this study we have introduced a vehicle tracking and long-term prediction method for dynamic urban scenarios. Object tracking is based on a representation of the environment relying on scene flow data combined with the image content. A two-stage mean-shift algorithm is used for detection of all moving objects in the scene. The first stage consists of an image-based mean-shift which utilises a grey value histogram as a target model and the second stage is used as a refinement of the object pose largely along the depth axis. The prediction step in the tracking system relies on flow-based, kinematic, and trajectory-based prediction methods, whose application depends on the length of the observed motion history. We compare the performance of the proposed tracking and long-term prediction approach with that obtained using other prediction stages. Using the kinematic prediction model leads to a similar tracking performance (fraction of the frames in which the vehicles are tracked) as obtained for the trajectory-based prediction, where for the long-term prediction the trajectory particle filter is clearly superior to the kinematic prediction method.

REFERENCES

[1] R. E. Kalman, "A new approach to linear filtering and prediction problems," *Transactions of the ASME Journal of Basic Engineering*, vol. 82, pp. 35–45, 1960.

[2] C. Hermes, C. Wöhler, K. Schenk, and F. Kummert, "Long-term vehicle motion prediction," in *Proc. IEEE Intelligent Vehicles Symposium*, 2009, pp. 652–657.

[3] B. Barrois, S. Hristova, C. Wöhler, F. Kummert, and C. Hermes, "3d pose estimation of vehicles using a stereo camera," in *Proc. IEEE Intelligent Vehicles Symposium*, 2009, pp. 652–657.

[4] V. Lepetit and P. Fua, "Monocular model-based 3d tracking of rigid objects: A survey," *Found. Trends. Comput. Graph. Vis.*, vol. 1, no. 1, pp. 1–89, 2005.

[5] A. Yilmaz, O. Javed, and M. Shah, "Object tracking: A survey," *ACM Comput. Surv.*, vol. 38, no. 4, p. 13, 2006.

[6] R. Melli, A. Prati, R. Cucchiara, and L. de Cock, "Predictive and probabilistic tracking to detect stopped vehicles," in *Application of Computer Vision, 2005. WACV/MOTIONS '05 Volume 1. Seventh IEEE Workshops on*, vol. 1, Jan. 2005, pp. 388–393.

[7] A. Barth and U. Franke, "Where will the oncoming vehicle be the next second?" in *IEEE Intelligent Vehicles Symposium*, 2008.

[8] M. Yokoyama and T. Poggio, "A contour-based moving object detection and tracking," in *2nd Joint IEEE International Workshop on Visual Surveillance and Performance Evaluation of Tracking and Surveillance*, Oct. 2005, pp. 271–276.

[9] X. Luo and S. M. Bhandarkar, "Tracking of multiple objects using optical flow based multiscale elastic matching," in *Dynamical Vision*, ser. Lecture Notes in Computer Science, vol. 4358. Springer Berlin / Heidelberg, 2007, pp. 203–217.

[10] D. Comaniciu, V. Ramesh, and P. Meer, "Kernel-based object tracking," *IEEE Transactions on Pattern Analysis and Machine Intelligence*, vol. 25, pp. 564–577, 2003.

[11] B. Heisele, "Motion-based object detection and tracking in color image sequences," in *Proc. of Asian Conference on Computer Vision*, Taipei, Taiwan, 2000, pp. 1028–1033.

[12] B. Schiele, "Model-free tracking of cars and people based on color regions," *Image and Vision Computing*, vol. 24, no. 11, pp. 1172–1178, 2006.

[13] H. Kollnig and H.-H. Nagel, "3d pose estimation by directly matching polyhedral models to gray value gradients," *International Journal of Computer Vision*, vol. 23, no. 3, pp. 283–302, June 1997.

[14] A. Ottlik and H.-H. Nagel, "Initialization of model-based vehicle tracking in video sequences of inner-city intersections," *International Journal of Computer Vision*, vol. 80, no. 2, pp. 211–225, 2008.

[15] S. Avidan, "Support vector tracking," *IEEE Trans. Pattern Anal. Mach. Intell.*, vol. 26, no. 8, pp. 1064–1072, Aug. 2004.

[16] R. Fraile and S. J. Maybank, "Vehicle trajectory approximation and classification," in *British Machine Vision Conference*, P. H. Lewis and M. S. Nixon, Eds., 1998.

[17] M. Yin, H. Zhang, H. Meng, and X. Wang, "An HMM-based algorithm for vehicle detection in congested traffic situations," in *Intelligent Transportation Systems Conference*, Sept./Oct. 2007, pp. 736–741.

[18] N. Johnson and D. Hogg, "Learning the distribution of object trajectories for event recognition," *Image and Vision Computing*, vol. 14, no. 8, pp. 609 – 615, 1996.

[19] N. Sumpter and A. Bulpitt, "Learning spatio-temporal patterns for predicting object behaviour," *Image and Vision Computing*, vol. 18, no. 9, pp. 697 – 704, 2000.

[20] W. Hu, X. Xiao, Z. Fu, D. Xie, T. Tan, and S. Maybank, "A system for learning statistical motion patterns," *IEEE Transactions on Pattern Analysis and Machine Intelligence*, vol. 28, no. 9, pp. 1450–1464, Sept. 2006.

[21] F. Stein, "Efficient computation of optical flow using the census transform," in *DAGM04*, 2004, pp. 79–86.

[22] F. Huguet and F. Devernay, "A variational method for scene flow estimation from stereo sequences," in *IEEE Eleventh Int. Conf. on Computer Vision*, 2007.

[23] H. H. Bock, *Automatische Klassifikation*. Vandenhoeck & Ruprecht, 1974.

[24] G. R. Bradski, "Real time face and object tracking as a component of a perceptual user interface," in *Proc. of the 4th IEEE Workshop on Applications of Computer Vision*, 1998, pp. 214–219.

[25] Y. Cheng, "Mean shift, mode seeking, and clustering," *IEEE Trans. Pattern Anal. Mach. Intell.*, vol. 17, no. 8, pp. 790–799, 1995.

[26] M. Vlachos, G. Kollios, and D. Gunopulos, "Elastic translation invariant matching of trajectories," *Mach. Learn.*, vol. 58, no. 2-3, pp. 301–334, 2005.

[27] B. K. P. Horn, H. M. Hilden, and S. Negahdaripour, "Closed-form solution of absolute orientation using orthonormal matrices," *J. Opt. Soc. Am. A*, vol. 5, no. 7, pp. 1127–1135, 1988.

[28] S. Thrun, W. Burgard, and D. Fox, *Probabilistic Robotics (Intelligent Robotics and Autonomous Agents)*. The MIT Press, September 2005.